CLM - P 522

CLM - P 522

UKAEA

Preprint

STABILITY LIMITS TO ION SOURCE OPERATION

A P H GOEDE
T S GREEN

CULHAM LABORATORY
Abingdon Oxfordshire

1978

CLM-P 522

STABILITY LIMITS TO ION SOURCE OPERATION

A P H Goede and T S Green

Culham Laboratory, Abingdon, Oxon, OX14 3DB, UK
(Euratom/UKAEA Fusion Association)

ABSTRACT

Experiments in which the anode area of an ion source is reduced, in order to enhance its ionisation efficiency, show there are limiting lower values to this area below which the ion source cannot be operated. By comparing plasma potential measurements with predictions derived from particle balance equations the phenomenon is shown to arise from the reversal in plasma potential. It can be explained by examining the conditions for the existence of an anode sheath, following the same arguments that lead to the derivation of Langmuir's criterion for the cathode sheath. Langmuir's criterion, together with the derived anode criterion, imposes boundaries to source operating parameters. Measurements were performed using a picket fence type ion source.

(Submitted for publication in Physics of Fluids)

January 1978

1. INTRODUCTION

In the design of high intensity ion sources, for application to neutral particle injection systems, the main programme objective is to build a plasma source providing large area uniformity at the extraction plane ($\approx$ 500 cm^2) generated with high electrical efficiency and gas utilisation. In plasmas generated by primary electron impact ionisation, the efficiency is dependent on the containment time of the ionising electrons which can be enhanced by either using magnetic fields, shielding the anode from direct primary electron collection, or by reducing the geometric area of the anode, producing the same effect. The first approach is being followed in, for example, the duopigatron sources [1], the second in the magnetic field free sources [2,3].

Since the application of magnetic fields in general worsens plasma uniformity and magnetic field free sources are not very efficient, hybrid configurations have been pursued recently in which the anode area is reduced by localised magnetic fields leaving a large volume of the ion source unmagnetised. As a result good combinations of uniformity and efficiency have been obtained. The most extensively developed sources of this kind are the periplasmatron [4] and the picket fence ion sources [5,6,7].

Although the determining role of effective anode area in electrical efficiency and gas utilisation is clearly indicated, very little is known as to what limit the anode area can be reduced. Indeed, adequate criteria for the design and evaluation of anode area do not exist.

For the cathode the situation is different, since it is known from the early studies carried out in the Manhattan project that the geometric area of the cathode cannot be reduced below a certain minimum without invoking instability of the source [8]. This criterion provides a boundary condition to source operating parameters. Theoretically the criterion derives from Langmuir's sheath criterion [9], which states that for a stable cathode sheath a certain minimum fraction of the ions produced should flow back to the cathode. Therefore, at a given ion production rate, depending on source efficiency, a minimum area for the cathode is determined. This criterion has been verified in a number of experiments [8,10,11].

Investigating the effects associated with anode area reduction, it became clear that here also source stability is the limiting factor. In earlier work by Martin in the field of ion thrusters it was inferred that an indicative parameter for plasma stability is the plasma potential. He observed experimentally

that for stability the plasma potential had to be positive with respect to anode potential [12]. Consider a source where the walls are biased to collect ions, then reduction of anode area tends to reduce the electron flux out of the system whereas the ion flux remains the same. Since the ion and electron fluxes must be balanced such as to maintain quasi-neutrality, the plasma potential will reduce accordingly. So in the end reduction of anode area will cause the plasma potential to become negative and hence the requirement of a positive plasma potential imposes a lower limit to the anode area.

In order to test the proposal that source stability is related to plasma potential we performed measurements on the parameter variations of the plasma potential, and compared these with the predictions derived from particle balance equations. The results, given in section 4, show good agreement. Subsequently the implication on these parameters of a positive plasma potential is compared with the measured stability thresholds. This is presented in section 5 and also shows satisfactory agreement. The question then remains why the plasma potential needs to be positive for source stability. An explanation has been sought in requirements for a stable anode sheath similar to the ones that lead to the cathode sheath criterion. In section 6 it is shown that for a stable electron sheath (negative plasma potential) ions must not penetrate the sheath. Since this cannot be realised in our configuration, a negative plasma potential will lead to instability.

Measurements have been performed in an ion source of the picket fence type [5,6,7] first developed by the Oak Ridge group. In this configuration the anode is shielded by magnetic fields localised very closely to the anode wall. The magnetic fields are generated by permanent magnets in multipole configuration. Thus our work is relevant to essentially field free ion sources only, although it may be extended to include magnetised plasmas when an expression for the effective anode area is derived.

2. EXPERIMENTAL ARRANGEMENT

A schematic diagram of the source is shown in Figure 1. A simple reflex source (monopigatron) has been modified by inserting a copper cylinder of 15 cm diameter and 15 cm length in between the extraction plane and the original anode (electrode 1). This cylinder is lined at the outside with permanent magnets which are arranged to form a 24-pole line cusp field, similar to that originally employed for the production of Q-plasmas [13,14].

The source can be operated with this cylinder as an anode (electrode 3, Figure 1) or with a simple non-magnetically shielded anode (electrode 1) or with a combination of the two. In our previous work [6,15] it has been shown that these cusp fields, concentrated in the vicinity of the anode wall, serve to reduce the area

of the anode. The effective anode area, or leakage aperture of the cusps, is shown to be approximately equal to the Larmor diameter of the primary ionising electrons. These findings are in accordance with earlier measurements performed by Leung et al. [16] under different experimental conditions and using different techniques.

The field strength of the magnets at the vacuum side of the anode wall is maximally about 800 G, decreasing exponentially in radial direction. At 2.5 cm from the wall the field has decreased to about 10 Gauss, leaving an almost field-free region of 10 cm diameter. Axially the field strength is constant over a length of 5 cm dropping to zero at the anode ends. In order to define the cusp length, shields have been inserted (electrodes 2 and 4) coaxially to the anode and biased 30 V negative with respect to cathode. By varying the length of these shields different cusp lengths can be established. The cusps being studied have lengths of 10 cm, 7 cm, 5 cm and 3 cm.

Electrodes other than the anode(s) are biased 30 V negative with respect to cathode, thus ensuring reflection of the primary ionising electrons and also enabling one to measure the ion flux to these electrodes.

The cathode is a simple bifilar wound tantalum wire of 1.5 mm diameter. All power supplies are voltage or current regulated, the current level at which the arc is operated being controlled by the filament heating current.

A small cylindrical Langmuir probe (0.2 mm diam, 2 mm long) is introduced 1 cm in front of the extraction plane. It is movable in radial direction. This Langmuir probe has been used to obtain data on electron temperature and plasma potential. The plasma potential was derived from the knee in the log-lin plot of the probe characteristic. In the evaluation we have subtracted the ion component by drawing a tangent to the ion saturation part of the probe characteristic and evaluated the current with respect to this tangent. This produces straight line dependencies for the thermal part of the electron velocity distribution over about one order of magnitude. Absolute accuracy in the plasma potential measurements is probably not much better than 1 V. Relatively, however, the data were reproducable within 0.2 V. In Figure 2 we show a typical example of a Langmuir probe curve together with an evaluation of plasma potential and electron temperature.

3. LIMITS TO ION SOURCE OPERATION

When we reduce the arc voltage of an ion source, keeping source pressure and filament heater current fixed, we observe a continuous decrease in arc current, represented by the familiar I-V characteristic of an arc discharge. This is illustrated in curve "a" of Figure 3. The horizontal part represents the space charge limited regime, the vertical part the emission limited regime [3,17].

When increasing the anode area, the shape of these curves remains essentially unaltered. Reducing the anode area, however, we meet conditions at which the I-V curve becomes discontinuous. A critical voltage appears at which the arc is disrupted, as is illustrated in curve "b," Figure 3. Below this voltage it is not possible to strike or maintain an arc. Experimentally curves "a" and "b" were obtained by using either electrode 1 (Figure 1) or the 7 cm cusp (electrode 3) as an anode without breaking the vacuum but simply changing electrical connections.

The value of the critical voltage is both a function of gas pressure and anode area. The observed relation for the stability boundary is illustrated in Figure 4 for three different cusp lengths: 7, 5 and 3 cm long. They clearly show an anode area dependence. The experimental procedure followed to obtain these curves is to set the gas flow rate at a definite value and then reduce the arc voltage until the arc extinguishes. Near threshold there is a sharp increase in fluctuation level of the ion flux to the biased walls. Normally it stays below a 1% rms value, but near threshold it increases above 10%.

For the 7 cm cusp no clear threshold is observed below 8 mTorr and for the 10 cm cusp a threshold did not appear at all. In these circumstances there is just a continuous decrease in arc current when decreasing pressure and voltage, similar to the large anode area case of curve "a," Figure 3. In section 5 it will be shown that this behaviour is characteristic for cathode area limitation.

Cathode area limitation has been studied extensively before by Bohm et al. [Ch.4,5 and 9 of Ref.8]. The relationship between minimum operating pressure and arc voltage, shown in Figure 9.94 of [8], bears resemblance to present curves in Figure 4. The difference is that present curves show a clear increase in stability threshold with reducing anode area, whereas this is not the case for cathode area limitation.

4. PLASMA POTENTIAL VARIATION

4.1 Particle balance equations

The plasma potential is determined by the requirement that ion and electron fluxes out of the system should equal their rates of production and maintain charge neutrality. Therefore an expression for the plasma potential follows from the particle balance equations. We assume that three distinct groups of particles exist in the discharge: primary ionising electrons, thermalised electrons and ions, and we assume furthermore that ionisation is caused by primary electrons only. This latter assumption, justified by the low values of the electron temperature measured, is discussed elsewhere in more detail [3, 18].

4.1.1 Primary electrons

The influx of primary electrons, represented by the arc current I_e, is either lost at the anode after a time τ_e or degraded in energy by inelastic collisions below the ionisation threshold after a time τ_{IN}. Since the walls are biased 30 V negative with respect to cathode potential, electrons are not lost at the walls. Hence:

$$\frac{I_e}{e} = \frac{n_b V}{\tau_e} + n_b n_o \langle \sigma v_b \rangle_{IN} V \qquad (1)$$

where n_b and v_b are the density and velocity of the primary electrons, n_o is the neutral gas density, V is the volume of the source and $\langle \sigma v_b \rangle_{IN}$ the reaction rate coefficient for inelastic collisions, averaged over the velocity distribution of the primary electrons.

4.1.2 Thermal electrons

Secondary electrons are produced as a result of energy degradation of the primaries and in the ionisation process. It is assumed that these secondary electrons thermalise rapidly whilst accumulating to a density which is orders of magnitude higher than the primary electron density. Because of their low temperature they have lost their ionising capability. We assume that initially the plasma potential is positive with respect to the anode and so the random flux of electrons which can overcome the sheath in front of the anode is given by Boltzmann's law:

$$n_b n_o \{ \langle \sigma v_b \rangle_{IN} + \langle \sigma v_b \rangle_{ION} \} V = \frac{1}{2\sqrt{\pi}} n_e v_e A_a \exp\left(-\frac{e\Phi}{kT_e}\right) \qquad (2)$$

where n_e and v_e are the thermal electron density and velocity, $v_e \equiv \left(\frac{2kT_e}{m_e}\right)^{\frac{1}{2}}$, A_a is the anode area for thermal electron collection, Φ is the plasma potential and T_e the electron temperature, e and m_e are the electron charge and mass, k is the Boltzmann constant.

4.1.3 Ions

Ions are created at a rate $< \sigma v_b >_{ION}$ and, in the case of a positive plasma potential, are lost to all electrodes after a time τ_+. The ion flux, as will be shown later, is determined by diffusion and so the ions possess a directed motion:

$$n_b n_o <\sigma v_b>_{ION} V = \frac{n_i V}{\tau_+} = \frac{I_+}{e} \qquad (3)$$

where n_i is the ion density and I_+/e is the total rate of ion production. The part of I_+ which is incident on the walls can be measured as a current. In equation (2) and (3) we have assumed that the number of neutral atoms is high enough that ionisation is not limited by arc starvation. This is allowed for the low values of arc current being considered.

In these equations the density of the particles should be such that charge neutrality is maintained: $n_e + n_b = n_i$ and, because the density of the primaries is very small, we may write:

$$n_e \tilde{\sim} n_i \qquad (4)$$

Dividing (2) through (3), using (4) leads to

$$\exp\left(\frac{e\Phi}{kT_e}\right) = \frac{1}{2\sqrt{\pi}} v_e \tau_+ \frac{A_a}{V} (1 + \beta)^{-1} \qquad (5)$$

where $\beta = \dfrac{< \sigma v_b >_{IN}}{< \sigma v_b >_{ION}}$.

This equation relates plasma potential to anode area, source pressure (via τ_+) and arc voltage (via β). A similar relation has been given before by Langmuir [9]. In his equation 45 he gives the parameter variation of plasma potential for a situation in which the walls are floating and direct loss of the primary electrons to the anode can be neglected (that is when $\tau_e > \tau_{ION}$).

4.2 Experimental verification

4.2.1 Arc voltage variation

When increasing the arc voltage from 30 to 120 V we measure an increase in plasma potential from 0 to about 1 V, whilst the electron temperature decreases from 2.5 to 2 eV. Data refer to the 10 cm cusp experiment at a pressure of 4 mTorr. From equation 5 we expect a straight line dependence with slope - 1 of $e\Phi/kT_e$ vs. $\log(1 + \beta)$. Data from two experimental runs in Figure 5, show good agreement. The cross-sections used in this graph have been derived following an experimental procedure outlined in reference 3. Briefly this method derives from the expression of the ionisation efficiency, obtained by division of equations 1 and 3 which

yields:

$$\frac{I_e}{I_+} = \frac{1}{n_o \tau_e \langle \sigma v_b \rangle_{ION}} + \beta \qquad (6)$$

This equation, which has proved its usefulness before [3, 18], shows that the intercept of the straight line dependence between ionisation efficiency and inverse gas pressure represents β. The variation of this intercept with arc voltage has been measured in the 10 cm cusp arrangement and is illustrated in Figure 6. The ion current I_+ measured is the current to electrodes 1, 2 and 4. For comparison, data from a different source having a geometrically defined anode area are also plotted [3].

4.2.2 Source pressure variation

When we increase the source pressure from 3 to 30 mTorr we observe an increase in plasma potential from 0.5 to 2 V whilst the electron temperature drops from 2.5 to 1 eV (arc voltage is 90 V). Although no explicit pressure dependence is given in equation 5, the variation obviously derives from the variation in ion containment time with pressure. At the prevailing pressures the mean free path for momentum transfer collision is smaller than the dimensions of the source and therefore the ion motion, governed by diffusion, will be dependent on source pressure.

Let us first be more specific about the momentum transfer collision cross-section of ions and neutrals. What we need to know is the combined effect of all randomising collisions including charge exchange acting on the ions in the discharge. These are probably best represented by mobility measurements. The mobility measurements of H^+ in H_2, given in [19], show a reduced mobility K_o = 10 cm^2 V/s at E/p ratios of about 100 V/cmTorr [Figure 19.41, ref.19]. Here p is the source pressure and E the electric field inside the plasma. From measurements of the radial variation in plasma potential we derive electric fields of 0.5 to 1 V/cm and therefore E/p values of about 100 V/cmTorr are relevant to our source conditions. Relating this mobility to the drift velocity and the collision cross-section via its definitions, we arrive at a value for the momentum transfer collision cross-section of H^+ in H_2 of $\sigma_{IN} = 4.7 \times 10^{-15}$ cm^2, which corresponds to a mean free path of 6 mm at 10 mTorr. At higher ratios of E/p the reduced mobility K_o may become even smaller, but adequate data are not available.

Species measurements [20] show that under our conditions of relatively low arc current the concentrations of $H^+ : H_2^+ : H_3^+$ relate approximately as 1:2:2, so rather than H^+ the other species are more abundantly present. However, from the mobility measurements of H_2^+, which are rather incomplete, and of H_3^+, given in [19], we do not expect results on mean free paths which are different by more than a factor three.

Since the ions have a directed motion with a drift velocity v_D we may modify equation 3 and 5 substituting the relation:

$$\frac{n_i V}{\tau_+} = n_i v_D (A_w + A_a) \approx n_i v_D A_w \qquad (7)$$

where A_w is the biased wall area and A_a the anode area for ion collection. The wall area is assumed to be much larger than the anode area, an assumption which will be discussed in section 4.2.3. From drift velocity measurements in hydrogen by Rose [21] it is known that at the prevailing E/p values the drift velocity varies as $v_D \propto (E/p)^{\frac{1}{2}}$. Since the space charge electric fields that can be sustained in a plasma are of order kT_e/eL, where L is the scale length over which the electric field extends, we may write:

$$\frac{\tau_+}{V} \propto \frac{1}{A_w} \left(\frac{p}{E}\right)^{\frac{1}{2}} = \frac{1}{A_w} \left(\frac{eL}{kT_e}\right)^{\frac{1}{2}} p^{\frac{1}{2}} = \left(\frac{2eL}{m_e}\right)^{\frac{1}{2}} \frac{p^{\frac{1}{2}}}{v_e A_w}$$

Substituting this expression in equation 5 we obtain

$$\exp\left(\frac{e\Phi}{kT_e}\right) = K \frac{A_a}{A_w} (1 + \beta)^{-1} (p^{\frac{1}{2}} - p_o^{\frac{1}{2}}) \qquad (8)$$

where K is a constant and p_o a small term arising from the non-zero intercept of the τ_+ vs. $(p/E)^{\frac{1}{2}}$ relation, resulting from inversion of Rose's data [21].

We have tested the pressure dependence given by equation 8 for the 10 cm and 7 cm cusp arrangement (Figure 7). Both sets of data show excellent agreement with the proposed $p^{\frac{1}{2}}$ dependence of the drift velocity.

In Figure 7 it may be noticed that the plasma potential has actually dropped to negative values. However, one should take into account that these probe data have been obtained relatively far away from the anode close to the negatively biased wall. When changing from the 10 cm cusp to the 7 cm cusp by extending the length of electrode 4 (Figure 1), we effectively increase the distance from probe to anode plane and, just as for the potential variation in radial direction, there may as well be a potential drop of a few volts over this distance in axial direction. Therefore, we expect that the absolute values of the plasma potential are in fact up to a few volts higher.

4.2.3 Anode area variation

The anode area can be changed by altering electrical connections in one particular geometry using either electrode 1 or electrode 3, or both as an anode (Figure 1). The procedure can be repeated inserting different cusp lengths and, in this way, we have measured the plasma potential variation for the 7 cm and 10 cm cusp arrangements. In evaluating these data a difficulty arises in that

we do not know the effective area of the cusp anode for collection of thermal electrons and ions. Assessment of these areas requires knowledge of the leakage aperture of the line cusps.

Recent measurements by Leung [16], performed in a similar picket fence magnetic field configuration but produced by current carrying conductors, show that the width of the aperture scales as a hybrid Larmor radius ρ_H where $\rho_H = (\rho_e \rho_i)^{\frac{1}{2}}$, ρ_e being the Larmor radius of the thermal electrons and ρ_i the Larmor radius of the ions. This result was inferred from the electron and ion saturation currents measured with a probe scanning behind the fence. The halfwidths of these profiles have been taken as a measure for the leakage aperture. These measurements deviate from earlier measurements and theory on the aperture width of the cusp fields as reviewed in [22], which predict a scaling with ρ_i, the ion Larmor radius.

Due to this uncertainty and because the results are not very different, we have based our calculation of the cusp leakage area on both assumptions. Numerical values are based on an electron temperature of 2 eV, and H_2 ions at a temperature of 0.1 eV. The ion temperature is not measured, but, because of the high collision frequency with neutrals, we have assumed T_i to be not very different from room temperature.

In Figure 8 the results of the plasma potential variation are illustrated and show reasonable agreement with equation 8 taking both assumptions on leakage aperture scaling into account. From these measurements, which are fairly indirect, it is difficult to infer whether ρ_i or ρ_H scaling prevails. We would rather emphasise that no agreement with equation 8 is obtained under the assumption that ions and thermal electrons are collected by geometric areas, that is to say the full area of electrode 3 in Figure 1. We therefore conclude that, besides confinement of primary electrons as shown earlier in [6,15], the cusp fields around the anode also provide ion and thermal electron containment. This is of importance for ion source development since the ion source efficiency is lowered when the ions are lost at the anode or wall rather than being directed to the extraction plane.

5. BOUNDARIES TO STABLE SOURCE OPERATION

5.1 Anode area limitation

From the parameter dependencies of plasma potential on source pressure, arc voltage and anode area, given by equation 8, we may now infer the implication of a positive plasma potential on these parameters. For $\Phi \geq 0$ the right-hand side of

equation 8 has to satisfy the relation:

$$\frac{A_a}{A_w} \geq \frac{1}{K\, p^{\frac{1}{2}}} (1 + \beta) \qquad (9)$$

where the small term p_o has been neglected for the pressure range considered.

Eq.9 yields a criterion for the minimum ratio of anode area to wall area required for stable source operation at given source pressure and arc voltage.

To verify equation 9 experimentally we have to show that the stability boundaries as illustrated in Figure 4 do satisfy this relation. Results are illustrated in Figure 9. Use has been made of the cross-section dependence on arc voltage as given in Figure 6.

For the 3 cm and 5 cm cusp arrangements, data show a good agreement with the predicted linear variation of the square root of minimum pressure against $(1 + \beta)$. For the 7 cm cusp the agreement is poor. It should be remembered, however, that in this case a stability threshold is present only at high pressures, and represents a transition regime.

The slope of the lines does not go to zero as predicted by equation 9. This may be qualitatively understood as arising from the fact that the ion containment time τ_+ does not go to zero as p goes to zero, which was already indicated in equation 8 by the term p_o.

A second prediction of equation 9 is that the slope of the lines varies as (A_a/A_w). Using values of A_a and A_w derived in section 4.2.3, the ratio of the slopes expected for the 3 cm, 5 cm and 7 cm cusps should be 1:1.9:2.8. Experimentally the slopes of the 3 cm and 5 cm cusp arrangements relate as $1:(2.4 \pm 0.4)$, which is in reasonable agreement considering the uncertainties in calculating anode and wall area. For comparison we have drawn a line of slope 2.8 for the 7 cm cusp data, corresponding to the slope expected from the anode to wall area ratios.

There is a problem in attaching practical value to equation 9 arising from the variation in intercept. However, in general one may say that anode area limitation comes into effect for the 7 cm cusp arrangement. In this case the anode to wall area ratio is $A_a/A_w = 2.1 \times 10^{-2}$, and the numerical value of the constant involved is $K = 1.6 \times 10^3 \left[\text{Torr}^{-\frac{1}{2}}\right]$. These numerical values substituted in equation 9 now provide design data for the anode and wall area of a particular ion source configuration. It also shows that for stability it is advantageous to reduce the wall area. This can be realised using a source concept as described in [7], where the entire source wall is shielded by a picket fence field and used as an anode. In this geometry the wall area is reduced to approximately the extraction area, which for an ion source is the minimum wall area one can obtain.

The pressure dependence in equation 9 originated from the variation in ion containment time with pressure. At pressures below 1 mTorr, when the ion motion becomes collisionless, one may anticipate this dependence to disappear. In this case the ion motion is described by Tonks-Langmuir's free fall theory and the velocity with which ions reach the sheath is given by Bohm's velocity:

$$v_B \approx 0.5 \ (kT_e/m_i)^{\frac{1}{2}}$$

Inserting this velocity in equation 5, using equation 7, the minimum anode area criterion modifies as:

$$\frac{A_a}{A_w} \geq \left(\frac{\pi m_e}{2m_i}\right)^{\frac{1}{2}} (1 + \beta) \qquad (10)$$

This condition puts a heavier restriction on the ratio of anode to wall area than equation 9. It therefore yields a stability criterion valid at all pressures.

5.2 Implication on ionisation efficiency

Since reduction of the anode area increases the primary electron containment time and since increase in primary electron containment time improves the ionisation efficiency, one may run into conflict with the requirements on source stability (equations 9 and 10) when aiming at higher ionisation efficiencies. Ideally the primary electron containment time τ_e should be longer than the time it takes for the primaries to be degraded in energy below the ionisation threshold. As an order of magnitude this happens after one ionisation collision time τ_{ION}. Therefore, ultimate ionisation efficiency is achieved when

$$\tau_e > \tau_{ION} \qquad (11)$$

In a field free source a simple relation exists for τ_e [3]:

$$\tau_e = \frac{4V}{A_b v_b} \qquad (12)$$

where A_b is the anode area for primary electrons. Since $\tau_{ION}^{-1} = n_o \langle \sigma v_b \rangle_{ION}$ relation 11 implies an upper limit for the anode area at given source pressure and arc voltage:

$$A_b < 4n_o V \frac{\langle \sigma v_b \rangle_{ION}}{v_b} \qquad (13)$$

In a field free source the anode area for primary electrons A_b is equal to the anode area A_a for thermal electrons. Hence combination of equations 10 and 13 yields the result that good ionisation efficiency under stable operating conditions can be achieved only when the source dimensions exceed certain

minimum values

$$\frac{V}{A_w} > \frac{1}{4n_o} \left(\frac{\pi m_e}{2m_i}\right)^{\frac{1}{2}} \frac{(1+\beta)}{\sigma_{ION}} \qquad (14)$$

Current neutral beam injectors require a source pressure of a few mTorr, hence for an arc voltage of 40 V or larger equation 14 predicts that source dimensions should be typically 10 cm or larger.

In a picket fence ion source the anode area for primary electrons is not equal to the anode area for thermal electrons. Assuming the leakage aperture for thermal electrons equal to an ion Larmor diameter (section 4.2.3), then the right-hand side of equation 14 should be multiplied by the factor $m_e v_b / m_i v_i$. Under normal conditions this does not alter the results of equation 14 to a great extent.

5.3 Cathode area limitation

The analysis given by Langmuir [9] of the current flow across the sheath in front of the cathode shows that for stability the current densities at the cathode boundary should obey the following relation:

$$\frac{J_e}{J_i} \leq \left(\frac{m_i}{m_e}\right)^{\frac{1}{2}} \qquad (15)$$

where J_e is the current density of the emitted electrons and J_i the current density of the ions at the filament boundary flowing from plasma to cathode. The equality sign refers to the case of maximum electron emission, ie the case where $E = 0$ at the filament boundary.

The implication of equation 15 is that it also leads to parameter limitations on source operation because J_i is a function of source pressure and arc voltage. When we assume the ions to move isotropically towards the walls we may replace current densities by currents

$$I_e = J_e A_c \quad \text{and} \quad I_+ = J_{ip} A_w \qquad (16)$$

where J_{ip} is the ion current density in the plasma. Since our filament is a cylindrical wire there are two effects by which the current density at the edge of the filament is enhanced over the current density inside the plasma. First the ion collecting area of the filament is larger than its geometrical area because of the double sheath surrounding it. In our case this sheath thickness is of the order of the filament radius. Second, the self-magnetic field of the filament tends to concentrate the ion flux towards the filament. Since the current density in (15) refers to the filament edge we obtain

$$J_i A_c = J_{ip} f_c A_c \qquad (17)$$

where $f_c A_c$ is the effective cathode area for ion collection. Hence equation 15 transforms into

$$\frac{I_e}{I_+} \leq f_c \left(\frac{m_i}{m_e}\right)^{\frac{1}{2}} \frac{A_c}{A_w} \qquad (18)$$

This equation shows that for a given rate of ion production the arc current is limited. Alternatively, for a given cathode area it imposes a minimum to the ionisation efficiency. Substituting next the expression for the ionisation efficiency (equation 6) we derive a criterion for the minimum operation pressure depending on cathode area:

$$\frac{1}{n_o \tau_e \langle \sigma v_b \rangle_{ION}} + \beta \lesssim \frac{1}{n_o \tau_e \langle \sigma v_b \rangle_{ION}} \leq f_c \left(\frac{m_i}{m_e}\right)^{\frac{1}{2}} \frac{A_c}{A_w} \qquad (19)$$

Here the term β may be neglected at the I_e/I_+ values where cathode area limitation applies ($I_e/I_+ \gtrsim 20$). Hence equation 19 yields:

$$n_o \geq \frac{1}{\langle \sigma v_b \rangle_{ION}} \frac{1}{f_c \tau_e} \left(\frac{m_e}{m_i}\right)^{\frac{1}{2}} \frac{A_w}{A_c} \qquad (20)$$

an expression which was derived previously by Green [10]. Similar expressions were derived earlier by Lejeune [11] and Bohm et al. [Ch.4,5 and 9 of Ref.8]. In order to verify this relation we measured at fixed gas flow rate the minimum arc voltage that is required to produce an arc of 4A. Experimental data for the 10 cm and 7 cm cusp are shown in Figure 10a. When plotting these data in terms of n_o vs. $\langle \sigma v_b \rangle_{ION}^{-1}$ they produce a linear relationship [Fig.10b] which is characteristic for cathode area limitation as has been shown before by Bohm [8] and Green [10]. Therefore we conclude that for the 10 cm and 7 cm cusp arrangements the stability boundaries are determined by the cathode area, albeit for the 7 cm cusp at low pressures only. The data indicate that under the operation conditions studied the factor $f_c \tau_e$ is independent of arc voltage. An explanation may be found in the increase of sheath area with arc voltage, an effect which is not included in the one-dimensional theory from which equation 15 derives.

5.4 Comparison between anode and cathode area limitation

From our experiments with the 7 cm cusp arrangement it appears that at low pressures the source operation is limited by cathode area, whereas at high pressures the anode area limitation takes over. An explanation of this phenomenon can be found by comparing the different cross-section dependencies characteristic for both limitations. Comparing equations 9 and 20 we notice that for a fixed geometry the minimum pressure should vary as $(1 + \beta)^2$ for the anode limitation and as $\langle \sigma v_b \rangle_{ION}^{-1}$ for the cathode limitation. In Figure 11 we have plotted these expressions involving cross-sections as a function of arc voltage. For the ionisation cross-section data

of the reaction $H_2 + e \rightarrow H_2^+ + 2e$ have been taken [23]. It follows that at high voltages the cross-section relevant to cathode limitation is larger, whereas at low voltages the cross-sections relevant to anode limitation dominates. Since low voltages correspond to high pressures it follows immediately that in a transition regime we are limited by anode area at high source pressure and limited by cathode area at low pressure.

Another comparison between anode and cathode area limitation may be inferred from their relation to the ionisation efficiency I_+/I_e. As for the cathode criterion it follows from Eq.18 that the ionisation efficiency must exceed a certain minimum level. For the anode criterion, on the other hand, it follows from Eqs.6 and 12 and the discussion in Sec. 5.2 that it may set an upper limit to the ionisation efficiency. Hence the ionisation efficiency of an ion source is bounded from below by the cathode sheath criterion and from above by the anode area criterion.

6. SHEATH STABILITY

As shown in the previous paragraphs the phenomenon of minimum anode area limitation is apparently related to a negative plasma potential. When the plasma potential reverses sign with respect to the anode the sheath in front of the anode starts reflecting ions and accelerating electrons, and therefore changes from an ion sheath into an electron sheath. This is opposite to the normal situation being considered in the particle balance equations of section 4. The question arises why it is, if at all, that in our situation formation of an electron sheath leads to unstable discharge conditions.

In discussing the stability of the anode sheath we may follow an approach similar to that of Bohm in deriving his criterion for the minimum velocity ions should have when entering an ion sheath [8], and similar to the treatment of Langmuir in his derivation of the requirements for a stable cathode or double sheath [9]. These derivations depend on the existence of a solution to Poisson's equation in the sheath for a given particle distribution at the edge of the sheath. Excellent reviews of these theories are given in the books of Chen [24] and Franklin [25].

Consider a plasma potential negative with respect to anode. Then in the sheath the potential should be increasing and we assume this to be monotonic. Inside the plasma we know from measurements of the radial variation of plasma potential that the potential is decreasing towards the wall. In fact this is what causes the ions to diffuse outwards imparting on them a drift velocity v_D, whose pressure dependence we have measured in section 4.2.2. Therefore at the sheath edge the ions possess a directed motion enabling them to penetrate the

sheath. Inside the sheath they are decelerated and eventually reflected. We assume the ion motion in the sheath to be collisionless. As for ion-neutral collisions this follows from the calculations in section 4.2.2. As for ion-ion collisions this holds up to densities of 10^{12} cm^{-3}. Electrons, on the other hand, are accelerated in the sheath and lost at the anode. Because this loss makes up only a small fraction of the total electron flux we may assume the electrons to maintain a Maxwellian velocity distribution. Therefore, the velocity distribution of the electrons in the sheath is an accelerated half Maxwellian. At the edge of the sheath we assume that quasi-neutrality $n_e = n_i = n$ exists.

Schematically the potential distribution anticipated in front of the anode wall is sketched in Figure 12. We have defined the potential $\phi(x)$ such that it is positive for all x. This definition differs from our previous definition of plasma potential, denoted by Φ, which represented the potential relative to the anode potential. We consider the problem to be one-dimensional and magnetic field free. This probably is a good approximation for particles moving along the cusp lines into the anode. Poisson's equation is given by

$$\frac{d^2\phi}{dx^2} = \frac{e}{\varepsilon_o}(n_e - n_i) \tag{21}$$

with boundary conditions $\phi(0) = 0$ and $\phi'(0) = 0$.

The particle densities to be substituted have been calculated in the Appendix. For the electron density $n_e(x)$ we find

$$n_e(x) = n(o)\exp\left(\frac{e\phi}{kT_e}\right) \operatorname{erfc}\left(\frac{e\phi}{kT_e}\right)^{\frac{1}{2}} \tag{22}$$

a result well-known from the collisionless theory of Q-machines [26]. For the ion density $n_i(x)$ we find

$$n_i(x) = n(o)\left\{1 - \frac{2e\phi}{m_i v_D^2}\right\}^{-\frac{1}{2}} \tag{23}$$

When making the substitutions:

$$\chi = \frac{e\phi}{kT_e} \; ; \quad \xi = x\left(\frac{n_e e^2}{\varepsilon_o kT_e}\right)^{\frac{1}{2}} \text{ and } M^2 = \frac{m_i v_D^2}{kT_e}$$

equation 21 transforms into a dimensionless equation

$$\chi'' = \exp\chi \operatorname{erfc}\chi^{\frac{1}{2}} - \left(1 - \frac{2\chi}{M^2}\right)^{-\frac{1}{2}} \tag{24}$$

with $\chi(0) = 0$; $\chi'(0) = 0$ and $\chi(\xi) \geq 0$ for all ξ. For $\chi = \frac{1}{2} M^2$ this equation shows a singularity brought about by the fact that the ions have their turning point at this value of χ, thus making their density infinite. This, of course,

is due to the assumption of monoenergetic ions. For $\chi > \frac{1}{2} M^2$ the ion term in equation (24) has to be zero. For an electron sheath where ions are not able to penetrate, which may happen in cases where the ions do not have a drift-velocity directed towards the anode, this term is zero throughout and equation (24) is replaced by

$$\chi'' = \exp \chi \operatorname{erfc} \chi^{\frac{1}{2}} \tag{25}$$

Equation (24) can be integrated once by multiplying each side by χ' which yields

$$\tfrac{1}{2}\chi'^2 = \exp \chi \operatorname{erfc} \chi^{\frac{1}{2}} + 2\left(\frac{\chi}{\pi}\right)^{\frac{1}{2}} - 1 - M^2 \left[1 - \left(1 - \frac{2\chi}{M^2}\right)^{\frac{1}{2}}\right] \tag{26}$$

This result implies that the right-hand side must be positive for all $\chi \neq 0$. For small χ (edge of the sheath) we may expand the right-hand side as

$$\chi - \frac{4}{3\sqrt{\pi}} \chi^{3/2} + \tfrac{1}{2}\chi^2 - \frac{8}{15\sqrt{\pi}} \chi^{5/2} + \cdots - M^2 \left[1 - 1 + \frac{\chi}{M^2} + \tfrac{1}{2} \frac{\chi^2}{M^4} + \cdots\right] \geq 0$$

which to lowest order yields

$$-\chi^{3/2} \geq 0 \ .$$

Since by definition χ should be positive, there is no χ satisfying equation (26) and hence no stable sheath is possible. In Figure 13 we have plotted the exact behaviour of the functions

$$\begin{aligned} F(\chi) &\equiv \exp \chi \operatorname{erfc} \chi^{\frac{1}{2}} + 2\left(\frac{\chi}{\pi}\right)^{\frac{1}{2}} - 1 \\ \text{and} \quad G(\chi) &\equiv M^2 \left[1 - \left(1 - \frac{2\chi}{M^2}\right)^{\frac{1}{2}}\right] \end{aligned} \tag{27}$$

the latter for $M^2 = 1$ and $M^2 = 2$. Clearly $G(\chi) > F(\chi)$ for all $\chi \neq 0$ and hence the right-hand side of equation (26) is negative definite. Only when $G(\chi) \equiv 0$, that is when ions are not penetrating the sheath (equation 25), is a solution possible.

The physical explanation for this effect is that for a negative plasma potential the potential gradient $\phi'(x)$ in the sheath should be positive. However, when ions enter the sheath they are decelerated and hence their density builds up. On the other hand, the electrons are accelerated, which reduces their density. Then from Poisson's equation (21) and the fact that $\phi'(0) = 0$ it follows that $\phi'(x)$ is negative inside the sheath contrary to the requirement of an increasing plasma potential. When, however, the ions do not penetrate the sheath, which for instance is the case when there is no density gradient, then $\phi'(x)$ is positive and a stable solution is possible.

7. CONCLUSION

Besides restrictions to stable ion source operation which are imposed by cathode area there are similar restrictions due to anode area. They derive from the requirement of a positive plasma potential which in turn follows from conditions for a stable anode sheath. The criterion sets lower limits to source pressure, arc voltage and anode area and, consequently, may set an upper limit to ionisation efficiency.

Because the minimum pressure for stability is proportional to the ratio of wall area to anode area it is advantageous to minimise wall area. Ideally this is achieved in devices which are shielded entirely by picket fence magnetic fields and may explain the low pressure operation of such devices [14]. However, in an ion source one wall must be left open for extraction. In such a geometry it is certainly advantageous to have the backplate shielded by a picket fence magnetic field, which reduces the wall area to essentially the extraction area.

The implication of the variation of plasma potential with anode and wall area is that part of the ions are contained by the picket fence field. This adds a second argument in favour of equipping the source backplate with picket fence fields. A source based on this concept has been built by Hemsworth and is described in [7].

ACKNOWLEDGMENTS

It is a pleasure to acknowledge the discussions with our colleagues at Culham, particularly R N Franklin, M F A Harrison, P J Harbour, R S Hemsworth and A R Martin. We are indebted to B Singh for building the probe equipment and N Buckley for constructing the ion source.

APPENDIX

The ion and electron densities to be substituted in Poisson's equation are

Ions

The continuity equation requires

$$n(0)v_D = n_i(x)v_i(x)$$

in which the ion velocity $v_i(x)$ is derived from conservation of energy:

$$\tfrac{1}{2}m_i v_i^2 = \tfrac{1}{2}m_i v_D^2 - e\phi$$

where v_D is the drift velocity of the ions when entering the sheath. Then in the sheath the ion density $n_i(x)$ becomes:

$$n_i(x) = n(0)\ \{1 - \frac{2e\phi(x)}{m_i v_D^2}\}^{-\frac{1}{2}} \qquad \text{(A1)}$$

where $\phi(x)$ is the sheath potential with respect to the potential at the edge of the sheath.

Electrons

The random flux of thermal electrons crossing the sheath is given by

$$n(0)\overline{v_x} = \frac{1}{\sqrt{\pi}}\, n(0)v_e \qquad \text{(A2)}$$

where v_e is the electron thermal velocity and $\overline{v_x}$ the average velocity in positive x-direction

$$\overline{v_x} = \frac{\int_o^\infty v_x dv_x \iint f_M dv_y dv_z}{\int_o^\infty dv_x \iint f_M dv_y dv_z} \qquad \text{(A3)}$$

where f_M is the Maxwellian velocity distribution:

$$f_M = \frac{1}{\pi^{3/2} v_e^3} \exp\{-\frac{v_x^2 + v_y^2 + v_z^2}{v_e^2}\} \qquad \text{(A4)}$$

This half Maxwellian is accelerated into the sheath. At potential $\phi(x)$ the velocity of each electron becomes

$$v_x'^2 = v_x^2 + \frac{2e\phi}{m_e} \qquad \text{(A5)}$$

which alters the velocity distribution as

$$f_M' = f_M(v_x', v_y, v_z)$$

Hence the average velocity of the accelerated half Maxwellian becomes:

$$\overline{v_x'} = \frac{a\int^{\infty} v_x' \, dv_x' \iint f_M' \, dv_y dv_z}{a\int^{\infty} dv_x' \iint f_M' \, dv_y dv_z} \tag{A6}$$

where $a = \left(\frac{2e\phi}{m_e}\right)^{\frac{1}{2}}$

Since $v_x dv_x = v_x' dv_x'$ which follows from A5, equation A6 yields

$$\overline{v_x'} = \frac{1}{\exp\left(\frac{e\phi}{kT_e}\right) \operatorname{erfc}\left(\frac{e\phi}{kT_e}\right)^{\frac{1}{2}}} \frac{v_e}{\sqrt{\pi}} \tag{A7}$$

where $\operatorname{erfc} z \equiv \frac{2}{\sqrt{\pi}} \int_z^{\infty} e^{-t^2} dt$

Using expression (A7) and (A2) in the flux conservation equation

$$n_e \overline{v_x'} = n(0)\overline{v_x}$$

we arrive at

$$n_e(x) = n(0) \exp\left(\frac{e\phi}{kT_e}\right) \operatorname{erfc}\left(\frac{e\phi}{kT_e}\right)^{\frac{1}{2}} \tag{A8}$$

which is the expression for the electron density in the sheath.

REFERENCES

[1] Morgan O B — Symp. Ion Sources, Brookhaven, BNL50310(1971) p.129.

[2] Ehlers K W, Baker W R, Berkner K H, Cooper W S, Kunkel W B, Pyle R V and Stearns J W. — J.Vac.Sci.Technol. 10 (1973) 922.

[3] Green T S, Martin A R, Goble C, Inman M — 7th Eur.Conf.Contr.Fus. and Pl.Phys., Lausanne (1975) 93.

[4] Fumelli M, Valckx F P G — EUR-CEA-FC-809 (1976)

[5] Stirling W L, Tsai C C, Ryan P M — Rev.Sci.Instr. 48 (1977), 533.

[6] Goede A, Green T S, Singh B. — 8th Eur.Conf.Contr.Fus. and Pl.Phys., Prague (1977), 114.

[7] Hemsworth R S — Culham Report CPNI-CUL(77)8.

[8] Bohm D — The characteristics of electrical discharges in magnetic fields. Ed. Guthrie A, Wakerling R K, McGraw-Hill. New York (1949)

[9] Langmuir I — Phys.Rev. 33 (1929) 954.

[10] Green T S — CLM-PR17 (1975)

[11] Lejeune C — Symp.Ion Sources, Brookhaven, BNL50310 (1971) p.27.

[12] Martin A R — Plasma Phys. 14 (1972) 123.

[13] Goede A, Brakenhoff G J — Plasma Phys. 12 (1970) 815
Phys.Rev.Lett. 27 (1971) 1044
Plasma Phys. 15 (1973) 977

[14] Limpaecher R, MacKenzie K R. — Re.Sci.Instr. 44 (1973) 726.

[15] Goede A, Green T S, Singh B. — To be published.

[16] Leung K E, Hershkowitz N, MacKenzie K R. — Phys.Fluids 19 (1976) 1045.

[17] Gabovich M D — Physics & Technology of Plasma Ion Sources Fizika i Tekhnika Plazmennykh Istochnikov Ionov (1972) Translation FTD-HT-23-1690-72.

[18] Green T S, Goede A, Martin A, Inman M, Singh B. — To be published.

[19] Massey H S W — Electronic & Ionic Impact Phenomena Vol.3 Slow collisions of heavy particles. Clarendon Press, Oxford (1971)

[20] Martin A R — Private communication.

[21] Rose D J — J.Appl.Phys. 31 (1960) 643.

[22] Spalding I — Advances in Plasma Physics, Vol.4. Ed. A Simon & W B Thompson, John Wiley (1971)

[23] Rapp D, Englander-Golden P. — J.Chem.Phys. 43 (1965) 1464, taken from A R Martin, CLM-R157 (1976)

[24] Chen F F — Introduction to Plasma Physics, Plenum Press, New York (1974)

[25] Franklin R N — Plasma Phenomena in Gas Discharges, Oxford University Press, Oxford (1976)

[26] van der Houven-van Oordt A J. — Thesis, Utrecht (1969)

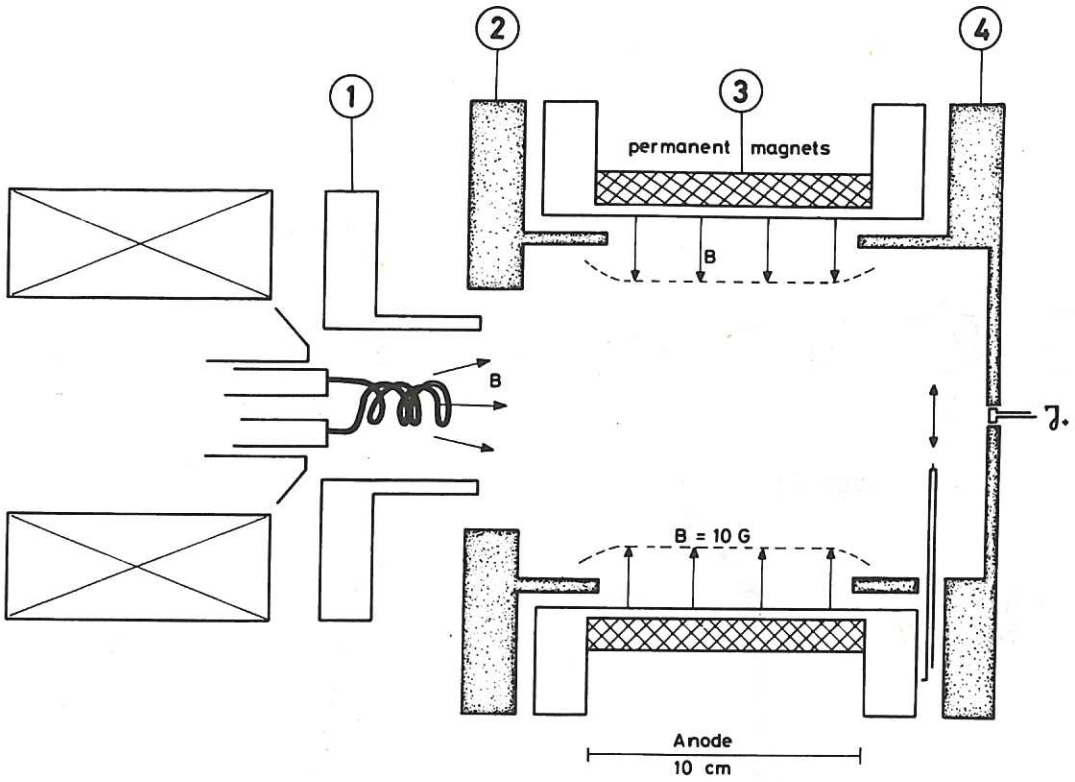

Fig.1a

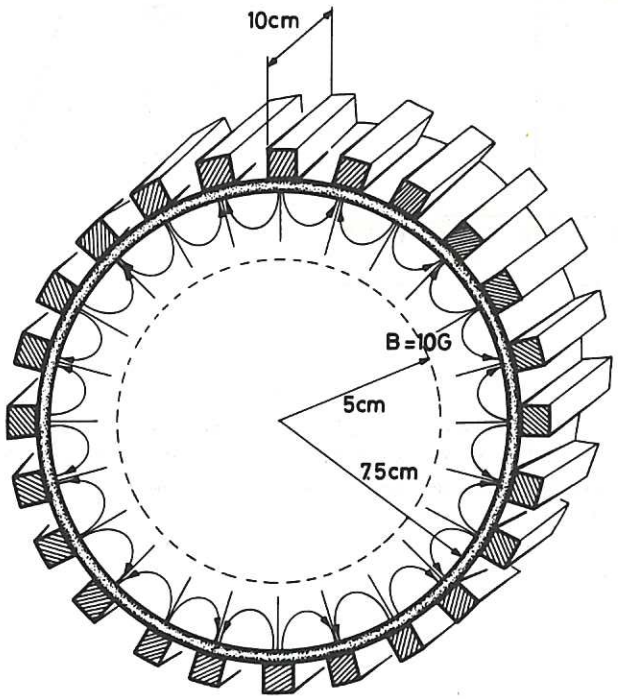

24-pole line-cusp

Fig.1b

Fig.1 Schematic of the picket fence ion source. Electrode (3), normally used as an anode, is shown in sectional view (Fig.1b). The anode area is reduced by the shielding action of a magnetic multipole field, generated by permanent magnets. The remaining electrodes are biased negative so as to confine the primary electrons. A cylindrical Langmuir probe is introduced in front of the extraction electrode (4). The solenoidal field coil shown has not been employed. The 10G contour indicates the boundaries of the almost field free volume in the source. All work has been done using hydrogen gas at pressures between 3 and 30mTorr.

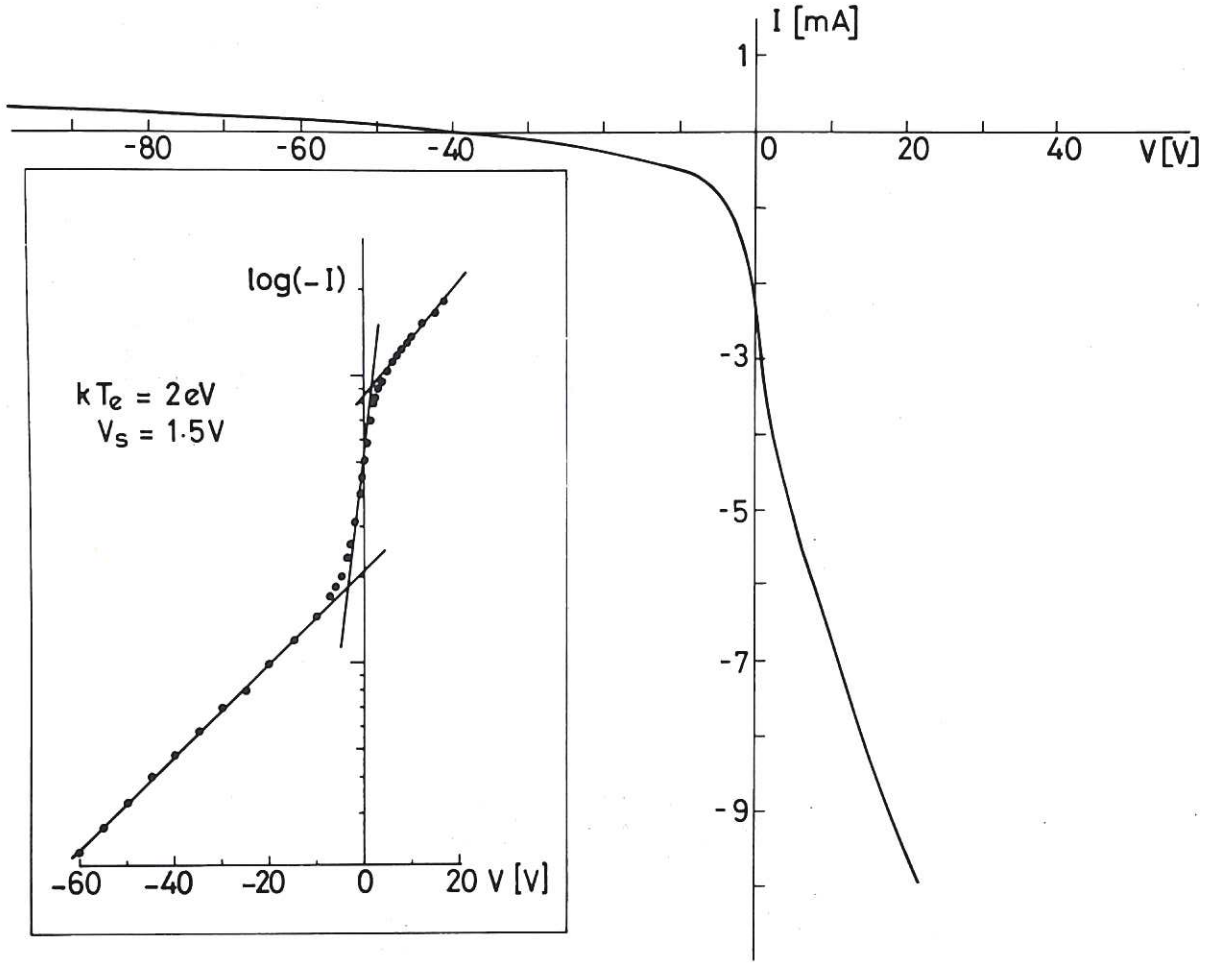

Fig.2 Current-voltage trace of a cylindrical Langmuir probe taken on axis near the extraction plane. In the evaluation the ion contribution has been substracted. Note the substantial contribution of primary electrons indicating they are the dominant ionising agent. The knee in the log-lin curve is taken as a measure of the plasma potential.

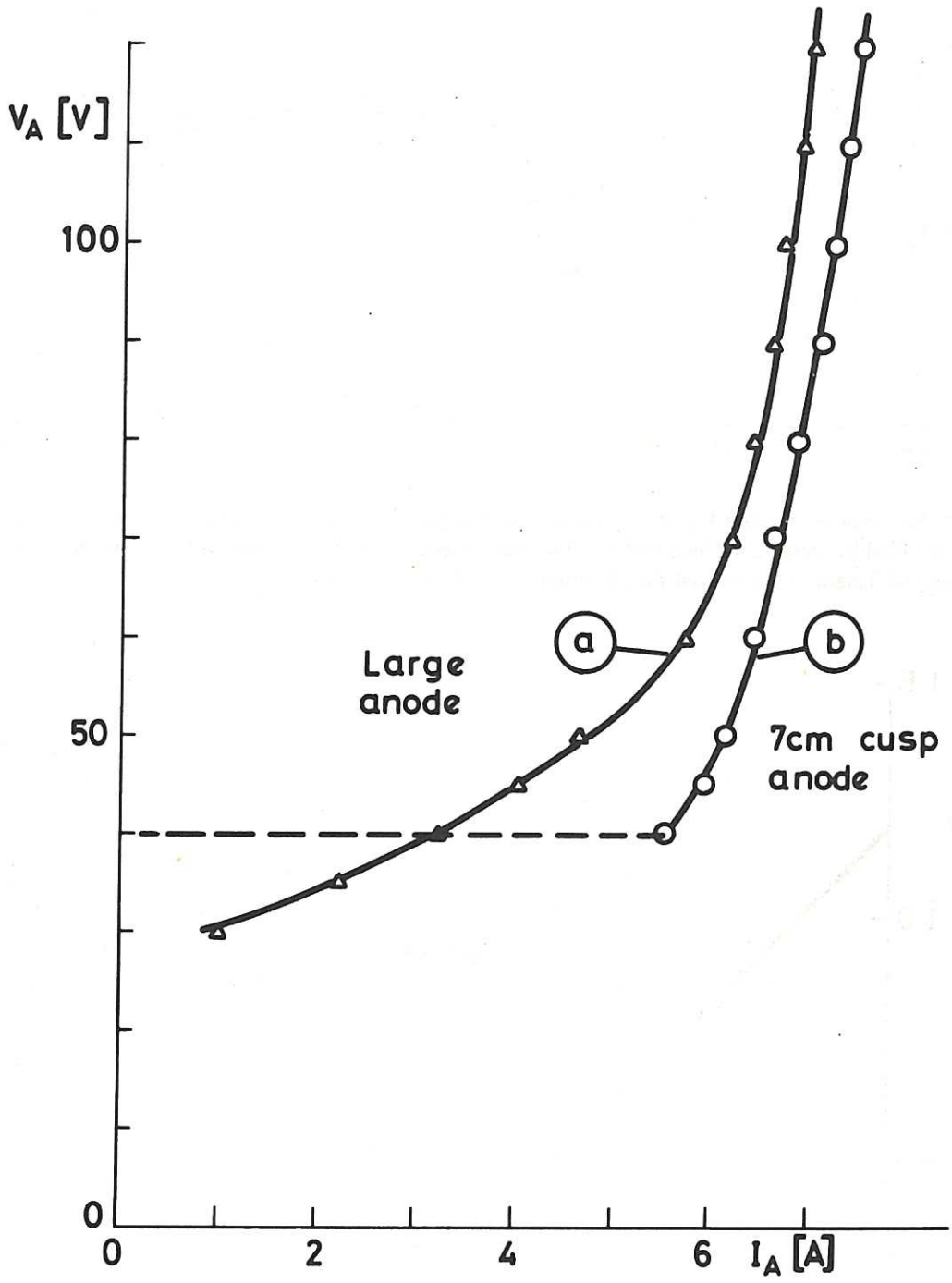

Fig.3 Current-voltage characteristic of the ion source measured by reducing arc voltage at fixed filament heater current. Curve "a" is obtained using electrode 1 (Fig.1) as an anode. Curve "b" represents the small anode case (electrode 3, Fig.1), illustrating the effect that source operation becomes impossible below a certain arc voltage when the anode area is very small.

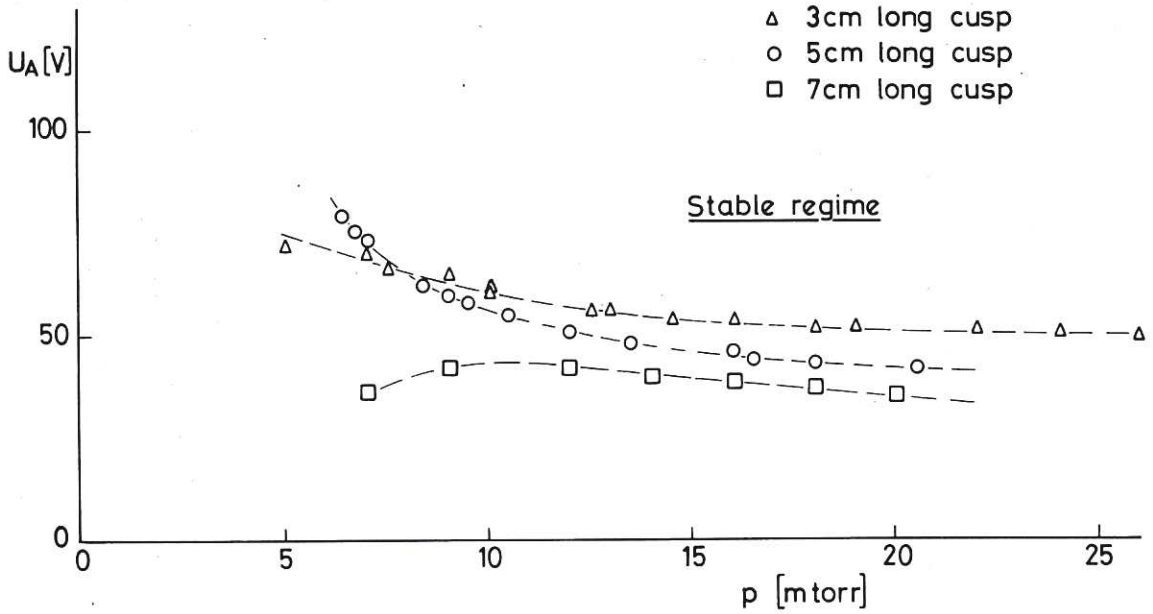

Fig.4 Minimum arc voltage U_A as a function of source pressure p for three different anode areas. The anode area is varied by altering the length of the line cusps (electrode 3, Fig.1). This has been accomplished by varying the length of the coaxial shields mounted on electrodes 2 and 4 (Fig.1).

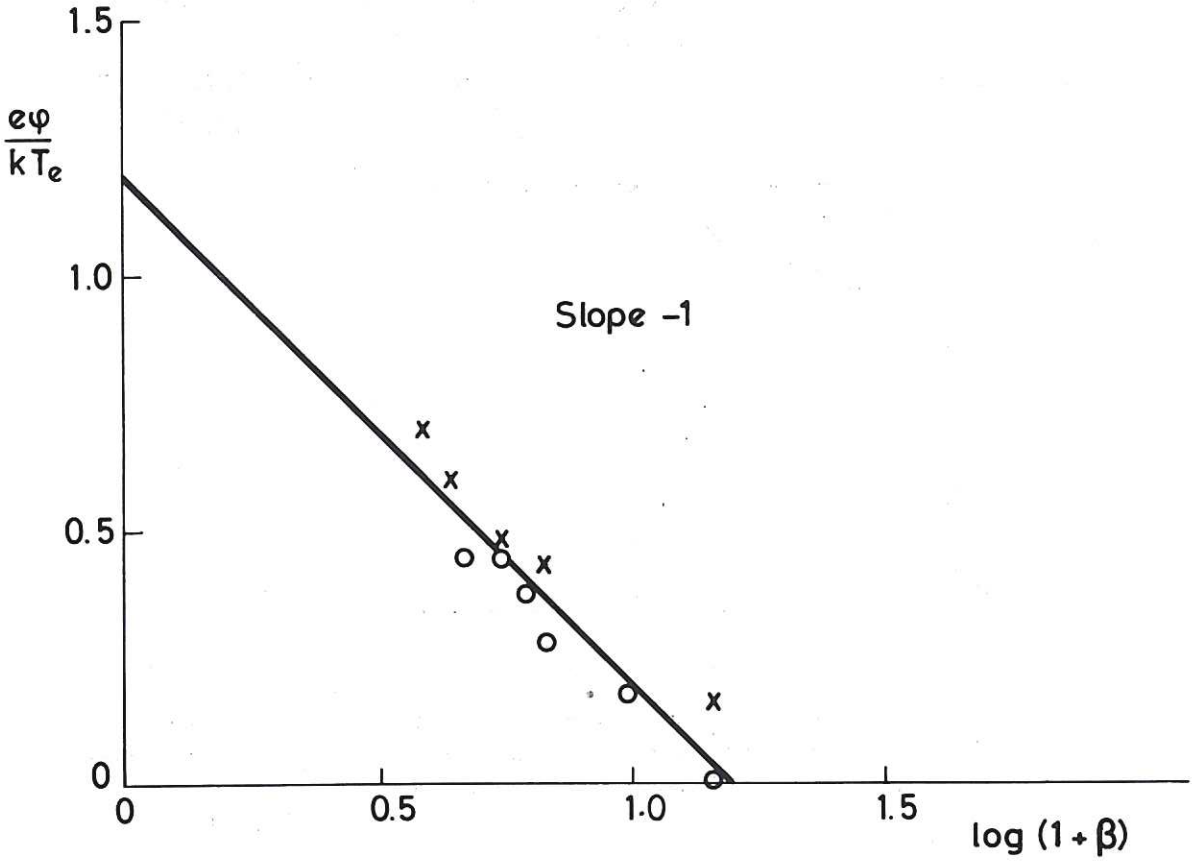

Fig.5 Variation of normalised plasma potential $e\Phi/kT_e$ vs. arc voltage via β, an expression involving cross-sections as defined in Eq.5. The line drawn is the prediction of Eq.5.

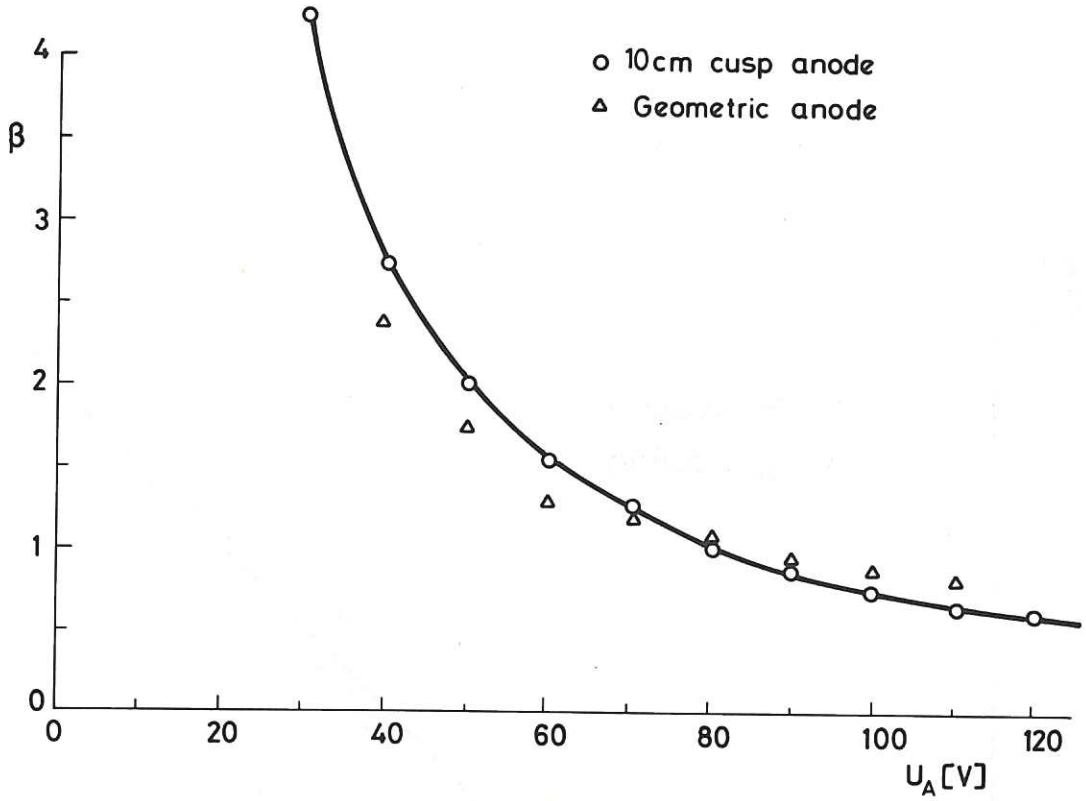

Fig.6 Variation of the cross-section term β vs. arc voltage, as derived from the intercept of the linear relation between inverse efficiency and inverse gas pressure (Eq.6). In evaluating these intercepts ion loss to the anode is supposed to be small, an assumption justified by comparing present data with those of previous experiments using a geometrically defined anode [Ref.3].

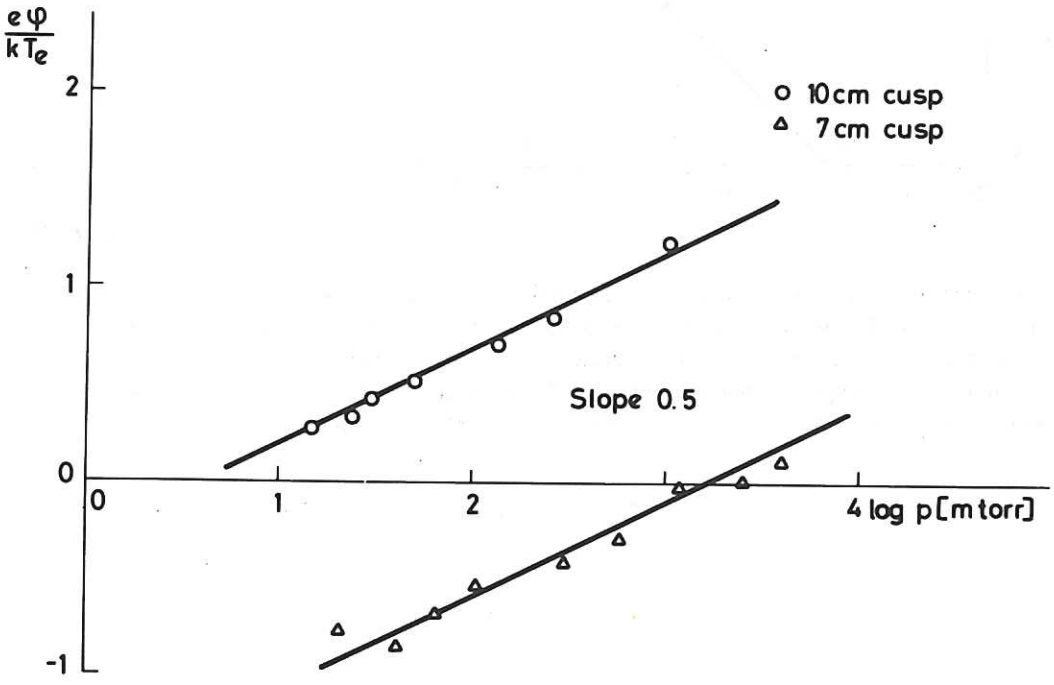

Fig.7 Variation of normalised plasma potential $e\Phi/kT_e$ vs. gas pressure p, as predicted by Eq.8. The pressure dependence arises from the variation in ion containment time with pressure. Data for the 7cm and 10cm long cusp arrangements are shown.

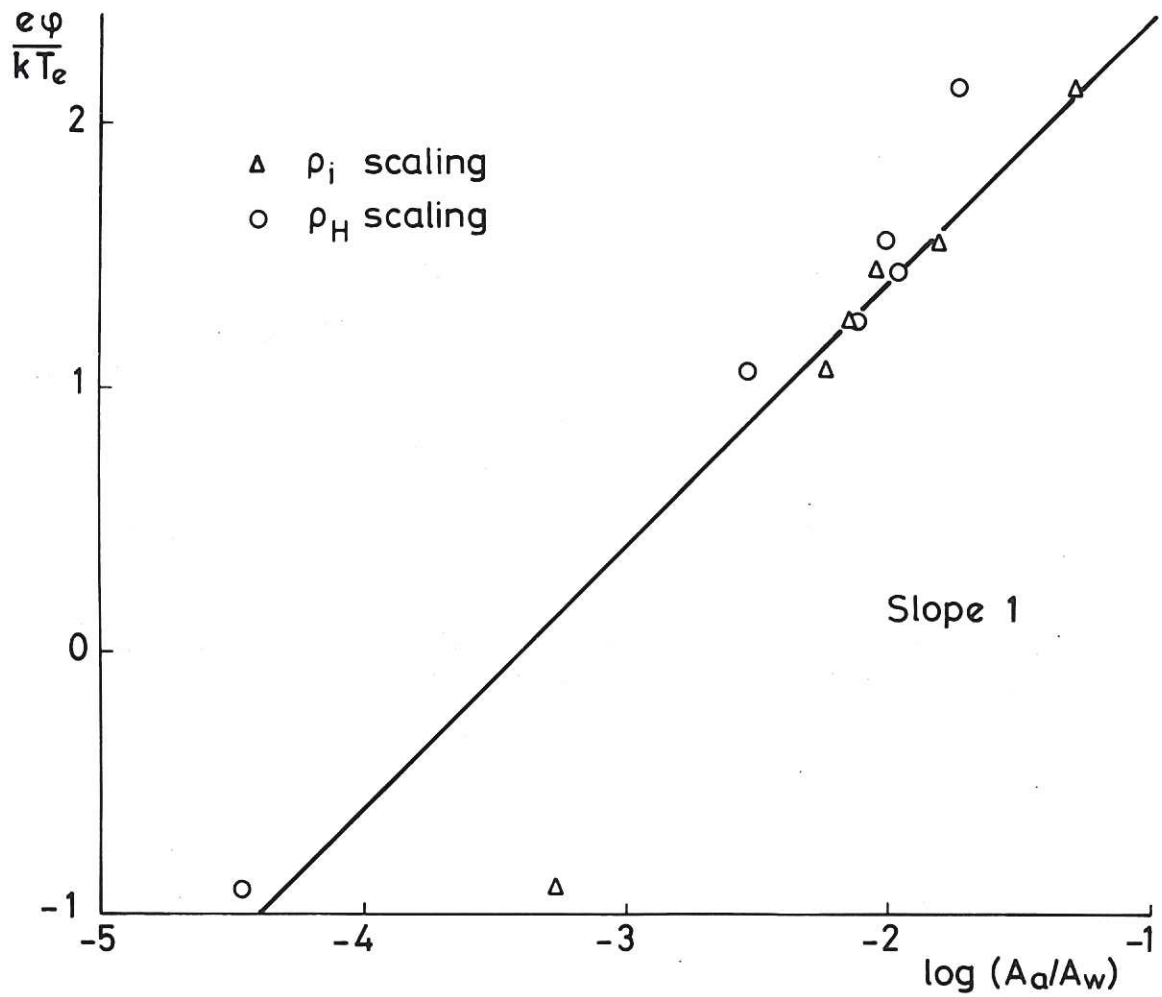

Fig.8 Variation of normalised plasma potential $e\Phi/kT_e$ vs. ratio of anode to wall area A_a/A_w as predicted by Eq.8. The anode area A_a has been varied by using either electrode 1 or electrode 3 or both as an anode (Fig.1), which yields three data points for each particular cusp arrangement. Data are shown for the 10cm and 7cm long cusp lengths. Triangles represent the assumption of ion Larmor diameter scaling of the cusp width whereas circles represent a hybrid Larmor diameter scaling.

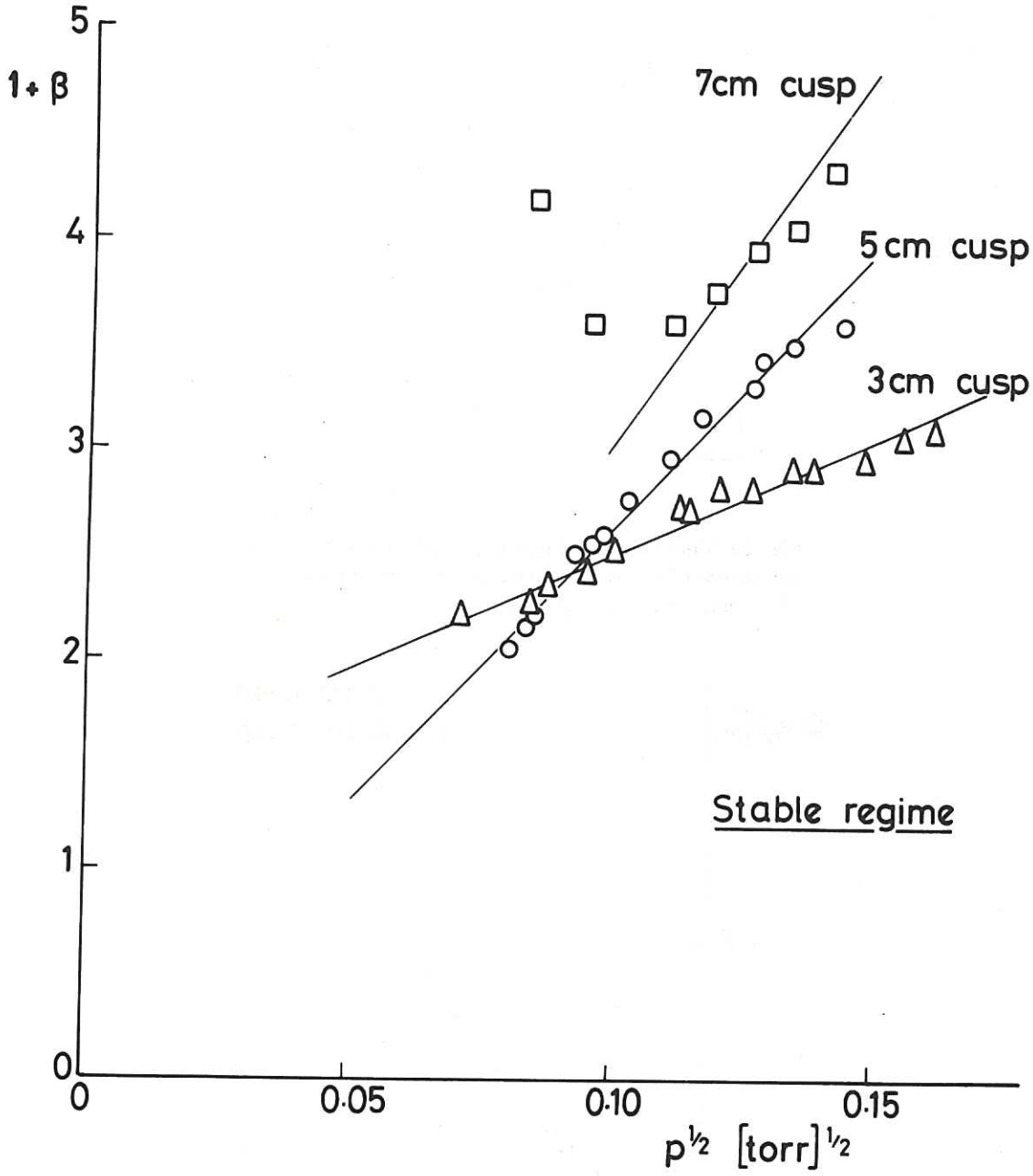

Fig.9 Boundaries to stable source operation as given in Fig.4, plotted in terms of the cross-section term $(1 + \beta)$ vs. the square root of gas pressure p. Lines indicate the predictions of Eq.9. Their slopes are varying approximately as the ratio of anode area to wall area A_a/A_w.

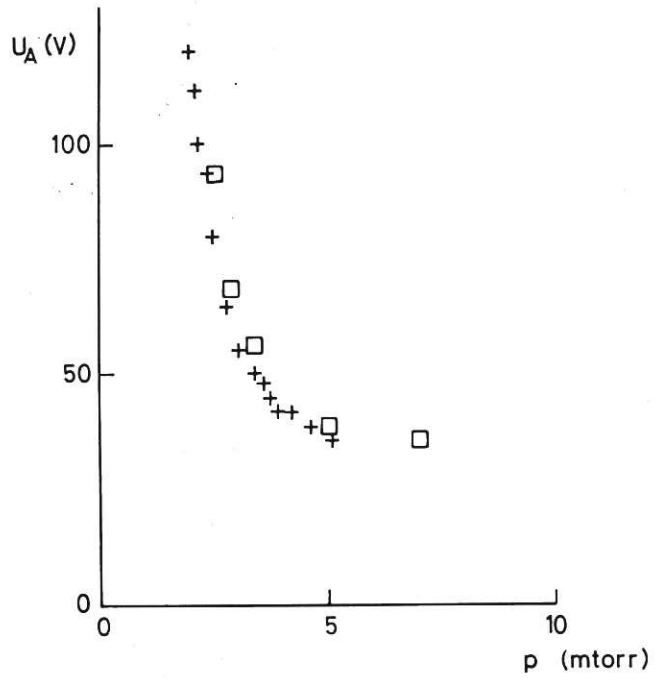

Fig.10a Minimum arc voltage U_A required to produce an arc current of 4 A as function of gas pressure p for the 10cm and 7cm long cusp length.

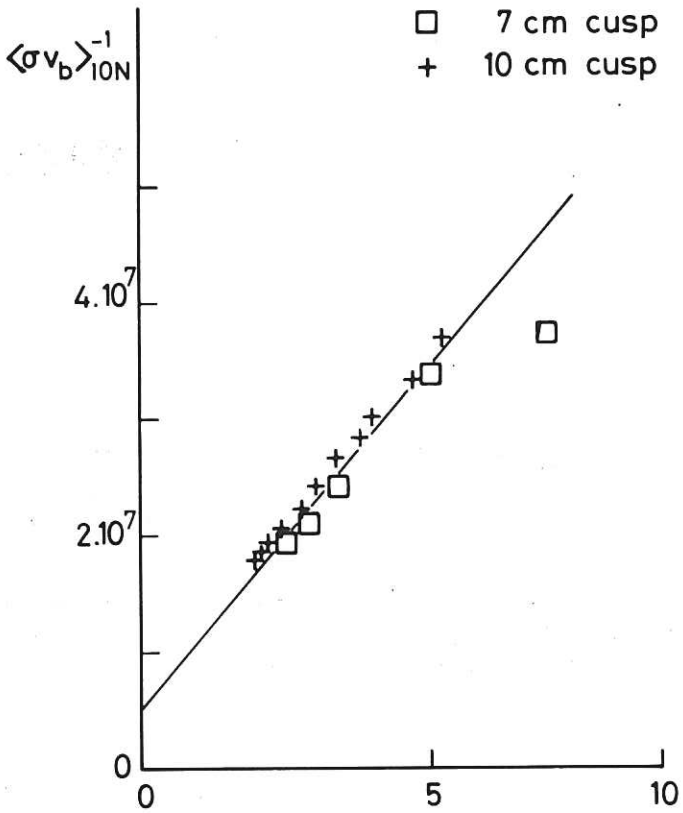

Fig.10b Data of Fig.10a have been plotted in terms of the inverse ionisation rate coefficient $\langle \sigma v_b \rangle^{-1}_{ION}$. They show the characteristic dependence of cathode area limitation as predicted by Langmuir's sheath criterion, Eq.20.

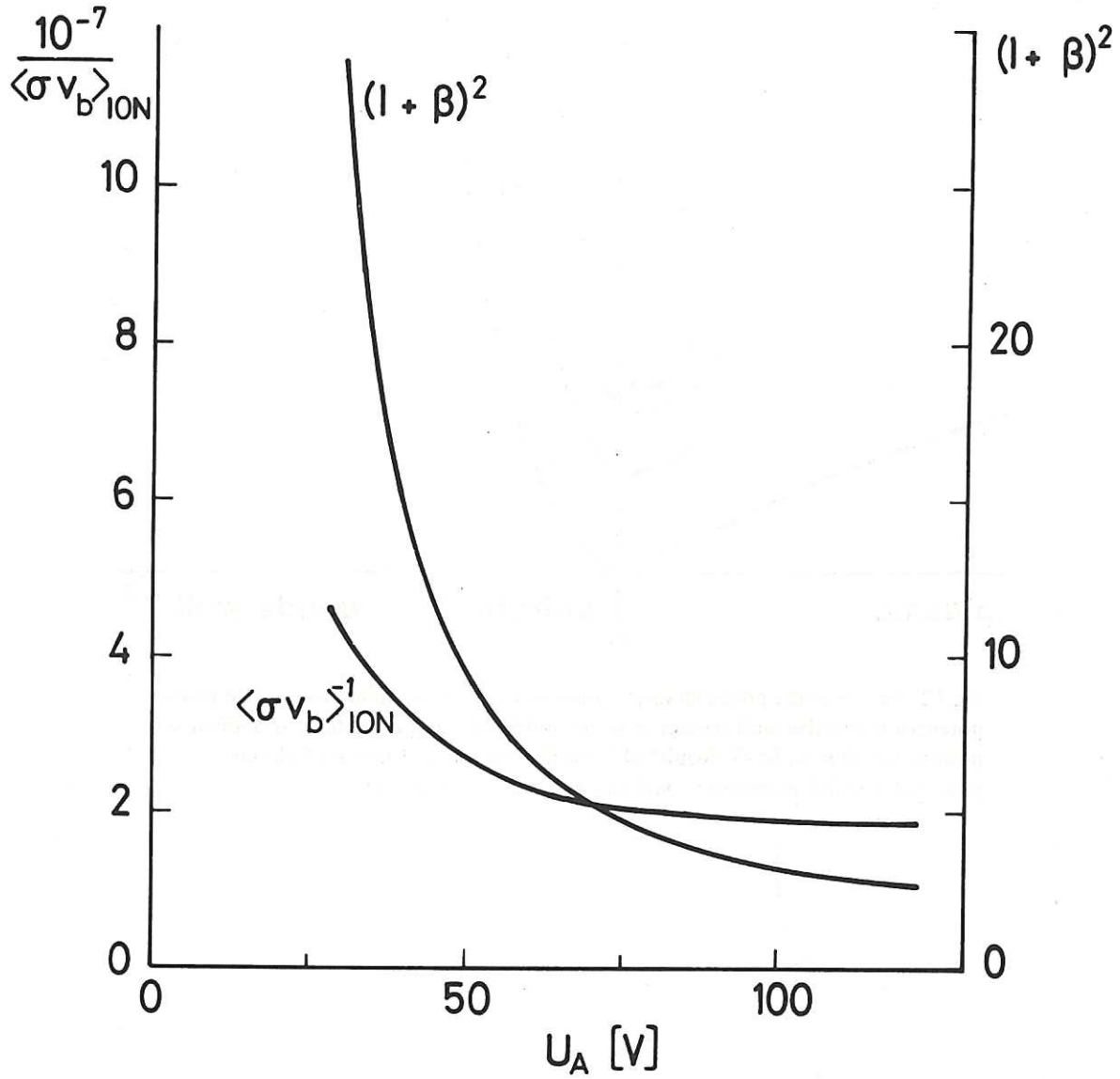

Fig.11 Variation with arc voltage U_A of terms involving cross-sections. The $\langle \sigma v_b \rangle^{-1}_{ION}$ variation is characteristic for cathode area limitation, whereas the $(1+\beta)^2$ dependence is typical for anode area limitation. At high arc voltages cathode area limitation dominates, whereas at low arc voltages anode area limitation takes over. See Eqs.9 and 20.

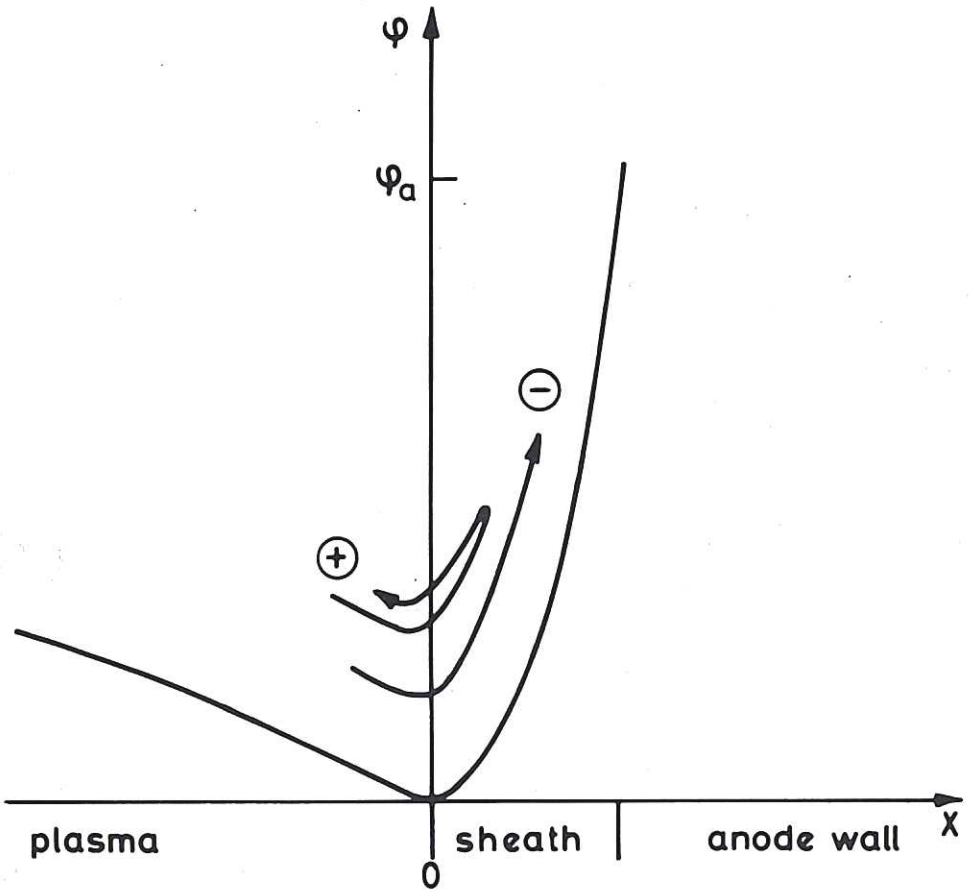

Fig.12 Sketch of the potential distribution in front of the anode in case the plasma potential is negative with respect to anode potential. The potential ϕ is defined as positive for all x, to be distinguished from the previous definition of plasma potential Φ which is measured with respect to anode potential.

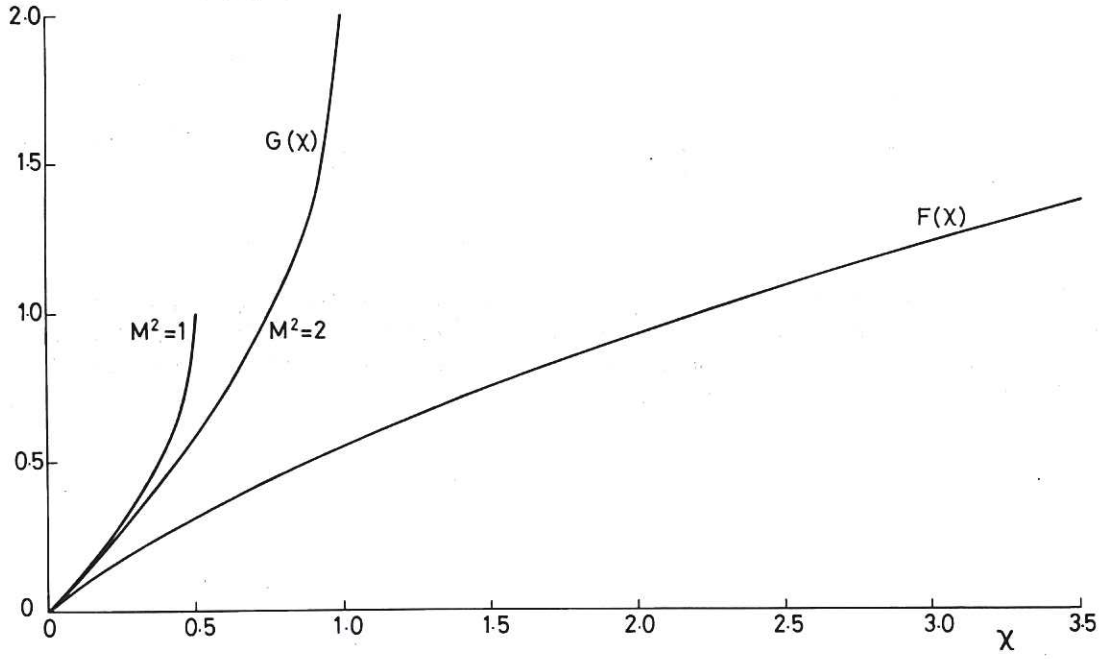

Fig.13 Theoretical variation of the functions $F(\chi)$ and $G(\chi)$, defined in Eq.27 and representing respectively functions of electron density and ion density as a function of the normalised potential $\chi = e\phi/kT_e$ as derived from integration of Poisson's equation. The difference of $F(\chi)$ and $G(\chi)$ is equal to the square of the normalised electric field represented by Eq.26.